Design of an fMRI-Compatible Optical Touch Stripe Based on Frustrated Total Internal Reflection

Behnaz Jarrahi[1,2], *Student Member, IEEE*, and Johann Wanek[3]

***Abstract*— Previously we developed a low-cost, multi-configurable handheld response system, using a reflective-type intensity modulated fiber-optic sensor (FOS) [1] to accurately gather participants' behavioral responses during functional magnetic resonance imaging (fMRI). Inspired by the popularity and omnipresence of the fingertip-based touch sensing user interface devices, in this paper we present the design of a prototype fMRI-compatible optical touch stripe (OTS) as an alternative configuration. The prototype device takes advantage of a proven frustrated total internal reflection (FTIR) technique. By using a custom-built wedge-shaped optically transparent acrylic prism as an optical waveguide, and a plano-concave lens to provide the required light beam profile, the position of a fingertip touching the surface of the wedge prism can be determined from the deflected light beams that become trapped within the prism by total internal reflection. To achieve maximum sensitivity, the optical design of the wedge prism and lens were optimized through a series of light beam simulations using WinLens 3D Basic software suite. Furthermore, OTS performance and MRI-compatibility were assessed on a 3.0 Tesla MRI scanner running echo planar imaging (EPI) sequences. The results show that the OTS can detect a touch signal at high spatial resolution (about 0.5 cm), and is well suited for use within the MRI environment with average time-variant signal-to-noise ratio (tSNR) loss $< 3\%$.**

I. Introduction

With an increasing popularity of magnetic resonance imaging (MRI), efficient and high performing devices that are compatible with use in an MRI setting are becoming more in demand. In recent years, interfaces with user-friendly and intuitive navigation options such as touch sensing found in small display devices (e.g., Apple's iPhone [2], and iPod touch [3]) and tabletop systems (e.g., Microsoft Surface [4], SMART Table [5], etc.) have become commonplace in everyday life. Several touch sensing mechanisms have been developed including resistive membrane [6], surface acoustic wave [7], piezoelectric [8], capacitive [9] and optical [10], [11] sensing techniques. However, utilizing such interfaces in MRI is still a challenge. The strong magnetic environment of the scanner limits the use of the conventional electromagnetic equipments. In addition, the current-carrying conductors are particularly liable to produce image artifacts by distorting the magnetic field homogeneity, especially when they are in the close proximity of the magnet [12], [13].

[1,2]B. Jarrahi is with the Department of Information Technology and Electrical Engineering, Swiss Federal Institute of Technology (ETH) Zürich, CH-8049 Zürich, Switzerland, and also with the Institute of Neuroradiology, University Hospital Zürich, CH-8091 Zürich, Switzerland; Phone: +41 44 255 56 03; (email: jarrahib@ethz.ch).

[3]J. Wanek is with the Spinal Cord Injury Center, Balgrist University Hospital, CH-8008 Zürich, Switzerland; (email: jwanek@paralab.balgrist.ch).

Among the available touch sensing approaches, optical touch sensing is more promising for implementation in MRI especially due to its inherent invulnerability to electromagnetic interference. But conventional optical touch systems primarily use infrared (IR) vision-based sensing which requires an IR imaging camera to be positioned in rear or in front of the touch surface for the direct line-of-sight to the objects being sensed [14]. Considering the characteristics of MRI environment, compatibility of electro-optical sensors have to be verified to avoid disturbance to the MRI system.

Although there are a few existing MRI-compatible touch pad systems (e.g. [15]), they are generally costly or still use electrical cables to communicate with the equipments outside the MRI scanner room. Accordingly, in this paper the design of a low-cost optical touch stripe (OTS) is presented. The sensing unit (Fig 1, top), which is completely free of electrical wires and ferromagnetic materials, is based on the optical detection of internally reflected light beams. Preliminary results show that it is MRI compatible and a technically feasible user interface for applications in fMRI.

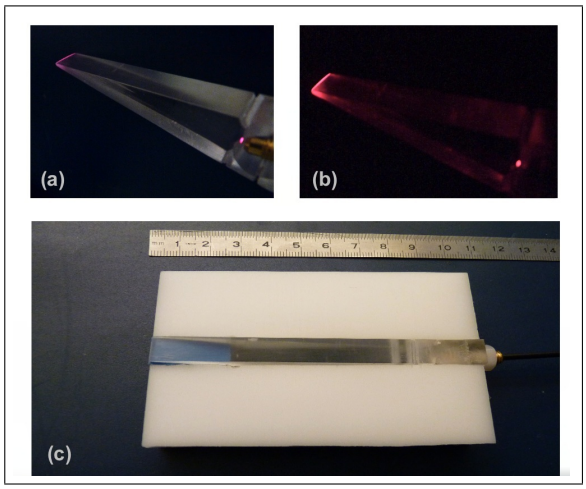

Fig. 1. The OTS prototype (a) with the light beams from a fiber-optic sensor illuminating the inside of the wedge-shaped acrylic prism in ambient light, (b) in the dark, and (c) with an integrated plastic base plate.

II. System Architecture

The OTS sensor is a reflective-type intensity modulated fiber-optic sensor (FOS) with a built-in light emitting diode (LED), and a flexible 10 m plastic-sheathed fiber-optic cable (FUE 500C1003, Baumer Electric, Switzerland). The FOS has a visible red light (centered at 680 nm) emitter element and a receiving element that are mounted side by side in a

978-1-4244-7929-0/14/$26.00 ©2014 IEEE

cylindrical brass housing (outer diameter 4.5 mm, length 24 mm) placed behind a custom-built plano-concave lens (focal length -10 mm and the radius of the lens aperture 5.0 mm). The lens is made of poly(methyl methacrylate) (PMMA, Plexiglas®, acrylic glass). When a beam of light is generated by the LED, it propagates down the optical fiber and emits into the air at the fiber tip. It then passes through the lens into an acrylic prism that is cast into a wedge-shaped structure with a dimension of 70 mm × 10 mm × T mm (with T from 20 to 2). The wedge prism is designed to have non-parallel front and back faces that are separated by a small angle $\alpha = 15^o$. The plano-concave lens is a divergent optical element and provides the required light beam profile by expanding the area covered by the LED. FOS receiving element receives reflections of light that become trapped within the prism. A rectangular plastic base plate (90 mm × 70 mm × 15 mm) with a narrow slot in the middle (85 mm × 10 mm × 15 mm) made of polyacetal copolymer (POM-C, Angst + Pfister, Switzerland) along with a polyamide M6 hex nut (Richco, USA) secures the prism, lens, and FOS in place as shown in Fig. 1 (bottom). The light beams illuminating the inside of the wedge prism through the lens can be seen in Fig. 1 (top panel). The technical specifications of the FOS are summarized in Table 1.

TABLE 1
SPECIFICATIONS OF THE OTS SENSOR

Parameter type	Specification
Sensing distance	25 mm
Light source	Pulsed red LED
Wave length	680 nm
Voltage supply range	10.8 to 26.4 VDC
Analog voltage output	1.0 to 5.0 VDC

The FOS is connected to a circuit board (Fig. 2) placed outside the MRI scanner room via a 10 m fiber-optic cable. This unit consists of a 15V AC-to-DC converter (PM10-15, Mean Well Inc., USA), a photodiode with an analog voltage output (FWDK 10U84Y0, Baumer Electric, Switzerland), and a data acquisition (DAQ) card (USB-6008, National Instruments, USA). The DAQ card is used as an interface between the optical sensing unit and a computer on which the operational software runs in conjunction with the OTS.

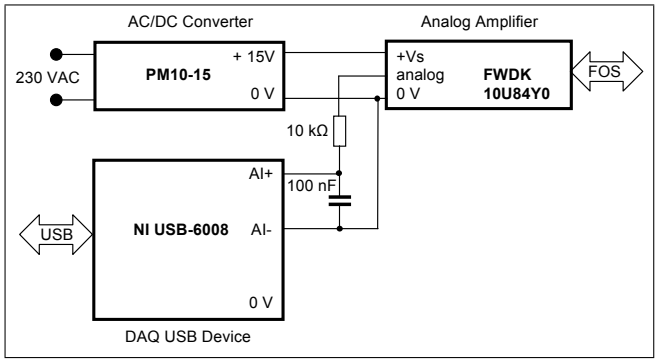

Fig. 2. The OTS circuit board including a power supply, data acquisition system, and an optical amplifier. A low-pass filter ($R = 10$ k, $C = 100$ nF) with a cut-off frequency $f_c = 159$ Hz is used to minimize noise.

III. PRINCIPLE OF OPERATION

The principle of operation of the prototype OTS is based on the frustrated total internal reflection (FTIR) caused by the difference in the refractive indices of the adjacent media. According to Snell's Law [16], when light passes from one medium to another with different refractive indices such that $n_1 > n_2$, total reflection of the incoming beam can occur at the interface between the two media if the angle of incident light beam (θ_i) exceeds a critical angle (θ_c) defined by (1):

$$\theta_i > \theta_c := \arcsin(n_2/n_1) \tag{1}$$

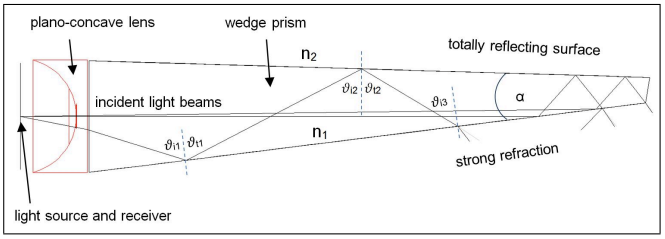

Fig. 3. 2D simulation of light beam propagation in an acrylic wedge prism through a plano-concave lens. The top surface acts as a touch-sensitive area where FTIR takes place while strong refraction occurs at the opposite face.

In the case of a light beam traveling through an acrylic wedge prism ($n_1 = 1.5$) into air ($n_2 = 1$), the critical angle for the total internal reflection to occur at the acrylic-air boundary is $\theta_c = 41.8^o$. Prisms can deviate light beams depending on how they are oriented relative to the input light, and how the prisms are cut. When the incident light beam enters an acrylic prism at an angle greater than its critical angle (i.e., $\theta_i > 41.8^o$), no refraction occurs in the wedge prism, and the light is totally internally reflected. By fabricating non-parallel front and back faces for the wedge prism that are separated by a small angle, total internal reflection of the light inside the wedge prism can be interrupted. An optimal range of $\alpha = 8.8^o$ to 23^o was estimated for wedge angle by running simulations with the WinLens 3D Basic software suite (Qioptiq, Germany). Sample 2D and 3D simulations are shown in Figs. 3 and 4. A final wedge angle $\alpha = 15^o$ was determined experimentally to be the best based on the characteristics of the FOS (Table 1), lens numerical aperture [17], and manufacturing techniques.

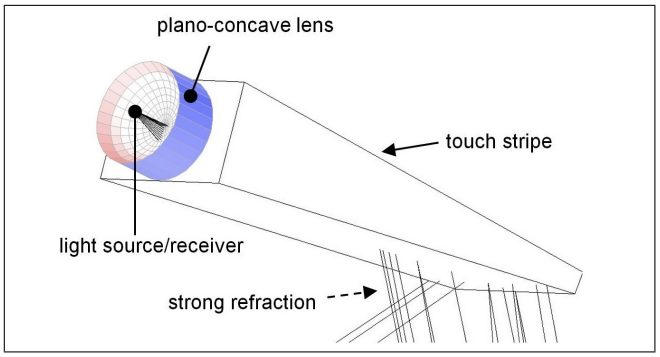

Fig. 4. 3D simulation of light beam propagation in an acrylic wedge prism through a plano-concave lens. FTIR phenomenon occurs at the top surface of the prism (i.e., *the touch stripe*, indicated by the black arrow) while strong refraction occurs at the opposite face (indicated by the dashed arrow).

This method traps the light inside the acrylic wedge prism, which is frustrated (scattered) at the point of a touch [11], [18]. The scattered light is then collected by a photodetector. As shown in Fig. 3, $\theta_{i_k} \geq \theta_{i_1} - \alpha(k-1) \geq \theta_c$ with the number of total reflections $k = \{1,2,3,...\}$, $\alpha \in [8.8^o\ ,\ 23^o]$, the reflection angle ($\theta_{i_k}$) decreases with increasing k. Thus, touching the surface of the acrylic wedge prism where FTIR phenomenon takes place (i.e., on the touch stripe) at a distance further away from the FOS leads to an increase in total internal reflections. This, in turn, generates greater output voltage signals that can be used to differentiate the position of a fingertip on the touch sensitive stripe area.

IV. Operational Software

The real-time operational software is implemented by using the National Instruments LabView™ software package (Austin, TX, USA), and several support modules written in C/C++, and Microsoft® Visual Basic (Microsoft Corporation; Redmond, WA, USA). The custom-written software runs on the IBM-compatible desktop computer (Dimension XPS 400; Dell Computer Corporation; Round Rock, TX, USA) connected to the MRI scanner PC to acquire output signals from the FOS, perform signal analysis, and display user interface data on a computer graphics monitor appropriate to a particular user task. For example, the software can translate the differences in output voltage from touching the OTS at different distances (Fig. 5 (a), (b)) as the position of a sliding bar along a vertical visual analog scale (VAS, which is widely used in fMRI as a graphic rating scale) ranging from 0 to 10 (Fig. 5 (c), (d)) or the pressing of a button in an array of push buttons (Fig. 5 (e), (f)).

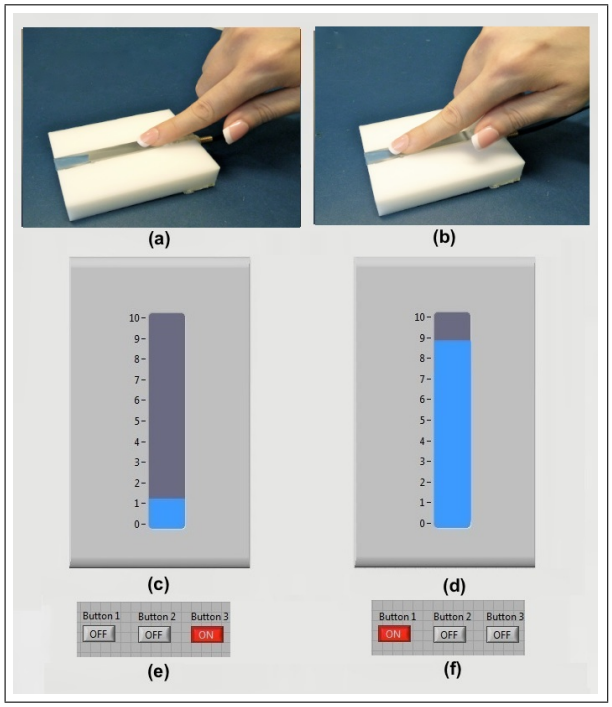

Fig. 5. (a) Difference in fingertip touch position results in different output voltage which is translated by the software to (c),(d) a position of a sliding bar on a VAS; or (e),(f) a depressed push button.

V. Performance Evaluation

To evaluate the accuracy of the fingertip position on the touch-sensitive stripe, we measured the intensity of the resultant internally-reflected light beams that were captured by the FOS receiving element and converted into an electrical signal by the photodiode. The amplified and low-pass filtered (refer to Fig. 2) output signal from the photodiode was measured with a digital multimeter (HP34401A, Hewlett-Packard, CO, USA). Fig. 6 shows a graph of percent output voltage versus position (distance) of the fingertip with respect to the FOS receiving element. The nonlinearity of the curve is caused by manufacturing tolerances of the handmade prism. The spatial resolution is obtained in the middle distance range by determining the smallest distinguishable output voltage difference (in this case 10 mV) at two adjacent touch positions. The value obtained is about 0.5 cm, which is comparable with the resolutions of conventional touchpad systems, ensuring even close-distance detection of touch signals from the user's fingertip.

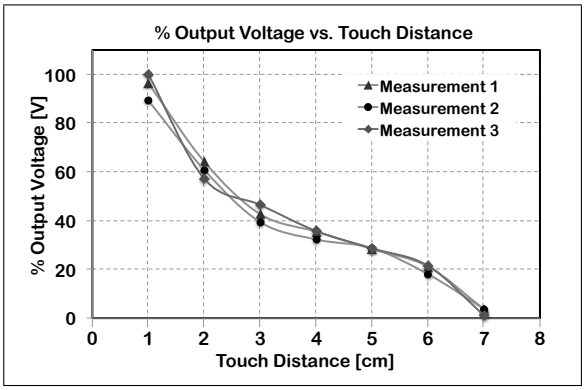

Fig. 6. Evaluation of the accuracy of fingertip touch position on the stripe

VI. MRI Compatibility Tests

A cylindrical homogeneous water phantom filled with 1.7 gram/liter of nickel chloride and 7 gram/liter of sodium chloride underwent echo-planar imaging (EPI) to investigate whether introducing the OTS to the MRI setting interfered with the signal during scanning. The phantom was scanned under four conditions: *(a)* without the presence of the OTS, *(b)* with the OTS present but turned off, *(c)* with the OTS present and turned on but not actuated, and *(d)* with an actuated OTS. All images were acquired on a 3.0 Tesla MRI system (Ingenia, Philips Healthcare, Best, The Netherlands) with 8-channel head-coil at the University Hospital Zürich. Images were acquired in an interleaved fashion with thirty four axial slices (each 3 mm thick, 1 mm interslice gap) using a gradient echo, echo-planar (EPI) $T2^*$-sensitive sequence (TR/TE = 2000/30 ms, FOV = 240 mm × 240 mm, image matrix = 96 × 96, voxel size = 3 mm × 3 mm × 3 mm, flip angle = 80°). We calculated the time-variant signal-to-noise ratio (tSNR) as a measure of image time course stability and degree of signal distortion during the scan (Fig. 7). tSNR is defined as the ratio between the temporal mean of a time series x_i and its temporal standard deviation [19]:

$$tSNR = \frac{\mu}{\sigma} = \frac{\mu}{\sqrt{\frac{1}{N}\sum_{i=1}^{N}(x_i - \mu)^2}} \quad (2)$$

where N is the number of time points, μ is the mean of the time series and σ is its standard deviation. As shown in Fig. 8, overall tSNR was decreased by no more than 3% across different fMRI compatibility test conditions.

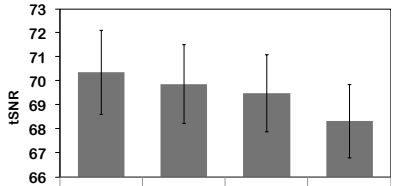

	Not present	Off	On	Actuated
Mean	70.37	69.88	69.50	68.33
SD	1.750	1.642	1.604	1.527

Fig. 7. Average tSNR for different fMRI compatibility test conditions

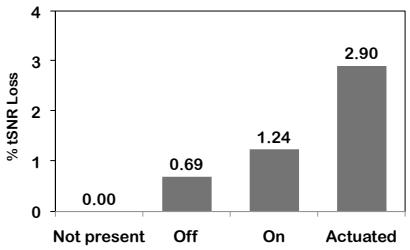

Fig. 8. Percent tSNR loss for different fMRI compatibility test conditions

We also evaluated the MR image quality with image subtraction method for each condition (Fig. 9). Changes from baseline (the phantom without the presence of OTS) were assessed by subtracting the absolute value between phantom image for that condition from the baseline image. Furthermore, upon visual inspection of all images and field maps, no noticeable image artifact associated with the presence of the device was observed. Likewise, no magnetically induced force or torque was observed when OTS was placed near the scanner bore (about 30 cm away from the phantom base) before and during the fMRI scans.

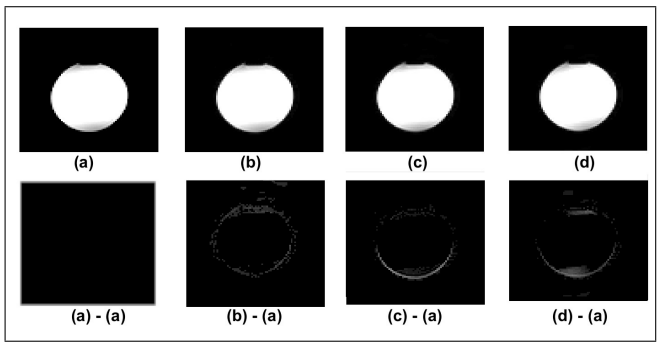

Fig. 9. (Top) A graphical representation of the imaging results; (Bottom) Image subtraction results with condition (a) as a baseline.

VII. Conclusion

We presented the design and architecture of a novel fMRI-compatible optical touch stripe as a feasible user interface to emulate physical push buttons or sliding bars during fMRI experiments. By taking advantage of the FTIR concept and using an intensity-modulated FOS, our device can accurately detect a touch signal from a user inside a 3.0 Tesla MRI scanner without a need for an IR sensor, an imaging camera, or any electronic components in close vicinity of the magnet. By adding an additional sensor element, it is possible to extend its functionality from 1D to 2D for, e.g., 2D tracking.

References

[1] B. Jarrahi, J. Wanek, U. Mehnert, and S. Kollias, "An fMRI-compatible multi-configurable handheld response system using an intensity-modulated fiber-optic sensor," in *Engineering in Medicine and Biology Society (EMBC), 2013 35th Annual International Conference of the IEEE*. IEEE, 2013, pp. 6349–6352.

[2] Apple iPhone, Available at http://www.apple.com/iphone/ [Last accessed on March 15th, 2014].

[3] Apple iPod touch, Available at http://www.apple.com/ipod/ [Last accessed on March 15th, 2014].

[4] Microsoft Surface Tablets - The Windows Tablet That Does More, Available at http://www.microsoft.com/surface [Last accessed on March 15th, 2014].

[5] SMART Table®442i collaborative learning center, Available at http://smarttech.com/table [Last accessed on March 15th, 2014].

[6] R. Bourdelais, R. Cok, and C. Kaminsky, "Flexible resistive touch screen," Oct. 28 2004, United States Patent App. 10/422,583. [Online]. Available: http://www.google.com/patents/US20040212599

[7] R. Adler and P. J. Desmares, "An economical touch panel using saw absorption," *Ultrasonics, Ferroelectrics and Frequency Control, IEEE Transactions on*, vol. 34, no. 2, pp. 195–201, 1987.

[8] R. S. Dahiya, G. Metta, M. Valle, A. Adami, and L. Lorenzelli, "Piezoelectric oxide semiconductor field effect transistor touch sensing devices," *Applied Physics Letters*, vol. 95, no. 3, p. 034105, 2009.

[9] P. Kalendra and W. Piazza, "Automatic calibration of a capacitive touch screen used with a fixed element flat screen display panel," Feb. 1 1994, United States Patent 5,283,559. [Online]. Available: http://www.google.com/patents/US5283559

[10] R. Doering, "Infrared touch panel," Sept. 19 1989, United States Patent 4,868,912. [Online]. Available: http://www.google.com/patents/US4868912

[11] J. Y. Han, "Low-cost multi-touch sensing through frustrated total internal reflection," in *Proceedings of the 18th annual ACM symposium on User interface software and technology*. ACM, 2005, pp. 115–118.

[12] K. Chinzei, R. Kikinis, and F. A. Jolesz, "Mr compatibility of mechatronic devices: design criteria," in *Medical Image Computing and Computer-Assisted Intervention–MICCAI'99*. Springer, 1999, pp. 1020–1030.

[13] G. Schaefers and A. Melzer, "Devices and materials in MRI," *Springer Handbook of Medical Technology*, pp. 503–521, 2012.

[14] S. Hodges, S. Izadi, A. Butler, A. Rrustemi, and B. Buxton, "Thinsight: versatile multi-touch sensing for thin form-factor displays," in *Proceedings of the 20th annual ACM symposium on User interface software and technology*. ACM, 2007, pp. 259–268.

[15] F. Tam, N. W. Churchill, S. C. Strother, and S. J. Graham, "A new tablet for writing and drawing during functional MRI," *Human brain mapping*, vol. 32, no. 2, pp. 240–248, 2011.

[16] M. Born and E. Wolf, *Principles of optics: electromagnetic theory of propagation, interference & diffraction of light*. CUP Archive, 1999.

[17] H. P. Zappe, *Fundamentals of Micro-optics*. Cambridge University Press Cambridge, 2010, vol. 90.

[18] J. Schöning, P. Brandl, F. Daiber, F. Echtler, O. Hilliges, J. Hook, M. Löchtefeld, N. Motamedi, L. Muller, P. Olivier, *et al.*, "Multi-touch surfaces: A technical guide," 2008.

[19] K. Murphy, J. Bodurka, and P. A. Bandettini, "How long to scan? the relationship between fmri temporal signal to noise ratio and necessary scan duration," *Neuroimage*, vol. 34, no. 2, pp. 565–574, 2007.